Journal of Porous Materials (2019) 26:1027–1034
https://doi.org/10.1007/s10934-018-0700-6

Fabrication of Al_2O_3 aerogel-SiO_2 fiber composite with enhanced thermal insulation and high heat resistance

Shangyan Wen[1,2] · Hongbo Ren[2] · Jiayi Zhu[2] · Yutie Bi[2] · Lin Zhang[3]

Published online: 4 December 2018

Abstract
The thermal-resistance Al_2O_3 aerogels and Al_2O_3 aerogel-SiO_2 fiber composite by using inorganic aluminum salt as the precursor were synthesized by the sol–gel process. The method was straightforward, inexpensive, and safe. Furthermore, it was found that the as-prepared Al_2O_3 aerogel had high crystal phase transition temperature. As the heat treatment temperature increased to 900 °C, the crystal phase transition from γ-AlOOH to γ-Al_2O_3 occurred within the Al_2O_3 aerogel. Meanwhile, the Al_2O_3 aerogel-SiO_2 fiber composite exhibited high Young's modulus of tensile strength up to 6.59 MPa and low thermal conductivity at 35 °C (0.028 W/(m K)) and high temperature of 600 °C (0.033 W/(m K)). In addition, the results indicated that the Al_2O_3 aerogel-SiO_2 fiber composite had the moderate hydrophobic property as well as mechanical property.

Keywords Al_2O_3 aerogel-SiO_2 fiber composite · Inorganic aluminum salt · Thermal insulation · Thermal stability

1 Introduction

Nowadays, the energy saving and emissions reduction is an effective way to achieve social and economic sustainable development. Thermal-insulation materials can effectively reduce the heat loss in the process of generation, transmission, storage and using, and have been widely used in civil and military fields, such as industrial piping, construction, aerospace, thermal battery and fire-protecting suit [1–8]. Fibrous thermal-insulation materials, with the advantages of low density, low thermal conductivity, low specific heat capacity and low cost, are becoming the most promising materials used in thermal protection system. However, organic fibrous thermal-insulation materials have disadvantages at high temperature and flame retardance. To the contrary, inorganic fibrous thermal-resistance materials are good at high temperature and flame retardance. The common inorganic thermal-resistance fibers are mainly the glass fiber, aluminum silicate fiber, Al_2O_3 fiber, ZrO_2 fiber, carbon fiber, and SiO_2 fiber [9–17]. The SiO_2 fiber has a good application in thermal insulation due to its chemical stability, thermal stability and thermal resistance. Thus, the SiO_2 fiber is expected to be a new thermal-resistance material, but its thermal resistance, thermal stability and humidity resistance are still not so good for satisfying with the practical application, however, which can be further improved [18–23].

It has been reported that Al_2O_3 aerogels exhibited an excellent high temperature performance that maintaining initial structure and thermal insulation at elevated temperatures above 1300 °C [24–28]. Thus, Al_2O_3 aerogels gradually become the prominent material used in high temperature field [29–31]. In general, the preparation of Al_2O_3 aerogels was achieved by using the organic aluminum salt or inorganic aluminum salt as the precursor [32–37]. Commonly, the aerogels prepared by using organic aluminum salts,

Electronic supplementary material The online version of this article (https://doi.org/10.1007/s10934-018-0700-6) contains supplementary material, which is available to authorized users.

✉ Hongbo Ren
Renhb@swust.edu.cn

✉ Lin Zhang
zhlmy@sina.com

1 State Key Laboratory of Environment-friendly Energy Materials, School of Material Science and Engineering, Southwest University of Science and Technology, 621010 Mianyang, People's Republic of China

2 State Key Laboratory of Environment-friendly Energy Materials, School of Science, Southwest University of Science and Technology, 621010 Mianyang, People's Republic of China

3 Research Center of Laser Fusion, China Academy of Engineering Physics, 621900 Mianyang, People's Republic of China

such as aluminum alkoxide, as precursors had good formability and excellent performance [35]. However, organic aluminum salts usually had the high toxicity, easy hydrolysis and high requirement for experimental environment. Thus, using inorganic aluminum salts as raw materials not only reduced the cost of preparing Al_2O_3 aerogels but also solved the experimental environment resistance caused by organic aluminum salts. Baumann pointed out that the inorganic aluminum salts, such as $Al(NO_3)_3·9H_2O$ and $AlCl_3·6H_2O$, could be used as the precursors to synthesis pure Al_2O_3 aerogels combined with supercritical drying process [33]. However, there were few reports about the mechanism of Al_2O_3 gel preparation by using $Al(NO_3)_3·9H_2O$ as the precursor, but the mechanism would be meaningful for understanding the Al_2O_3 sol–gel process. Moreover, Zhang et al. impregnated Al_2O_3–SiO_2 sols into porous zirconia ceramics to improve the stability at high temperature and obtain high compressive strength (1.22 MPa) and low thermal conductivity (0.049 W/(m K)) via supercritical drying [38]. Nevertheless, the composite still had high thermal conductivity. Therefore, developing a new kind of inorganic SiO_2 fibrous composite material, which possesses low thermal resistance, high thermal stability and good humidity resistance, is of great significance.

In this work, pure Al_2O_3 aerogels by using inorganic aluminum salt as the precursor were first prepared via the sol–gel method by supercritical drying. The as-prepared Al_2O_3 aerogels had the high thermal resistance. Inspired by the high thermal resistant Al_2O_3 aerogels, in order to reduce thermal conductivity and improve heat resistance of SiO_2 fiber mat, the Al_2O_3 sol was immersed into SiO_2 fiber mat to obtain SiO_2 fiber mat reinforced by high thermal resistant Al_2O_3 aerogels. The Al_2O_3 aerogel-SiO_2 fiber composite had low thermal conductivity, high heat resistance, high mechanical property and good humidity resistance. Furthermore, the mechanism of Al_2O_3 gel preparation by using inorganic aluminum salt as the precursor was also discussed in detail.

2 Experiment

2.1 Reagents and chemicals

Ethanol (EtOH, AR), propylene oxide (PO, AR), $Al(NO_3)_3·9H_2O$ (AR) were purchased ChengDu Kelong Chemical Reagent Company. All these reagents were used as received and all solutions were prepared with deionized water (< 18 M Ω, produced by UP instruments).

2.2 Fabrication of pure Al_2O_3 aerogels and Al_2O_3 aerogel-SiO_2 fiber composite

As seen from Scheme 1, the synthesis processes of pure Al_2O_3 aerogels and Al_2O_3 aerogel-SiO_2 fiber composite were as follow. First, the precursor solution was prepared by mixing with $Al(NO_3)_3·9H_2O$, EtOH and deionized water as the molar ration of 2:30:11.1 in a beaker under magnetic stirring at room temperature for 50 min. Then, the desired amount of PO was poured into the above solution, quickly stirred for 3 min, and transferred into the plastic molds to form wet gel. After aging at room temperature for 24 h, the wet gel was soaked in a absolute ethanol bath in 60 °C for 3 days to exchange the water and residual reagent from the pores of the matrixes. Then, the pure Al_2O_3 aerogels were

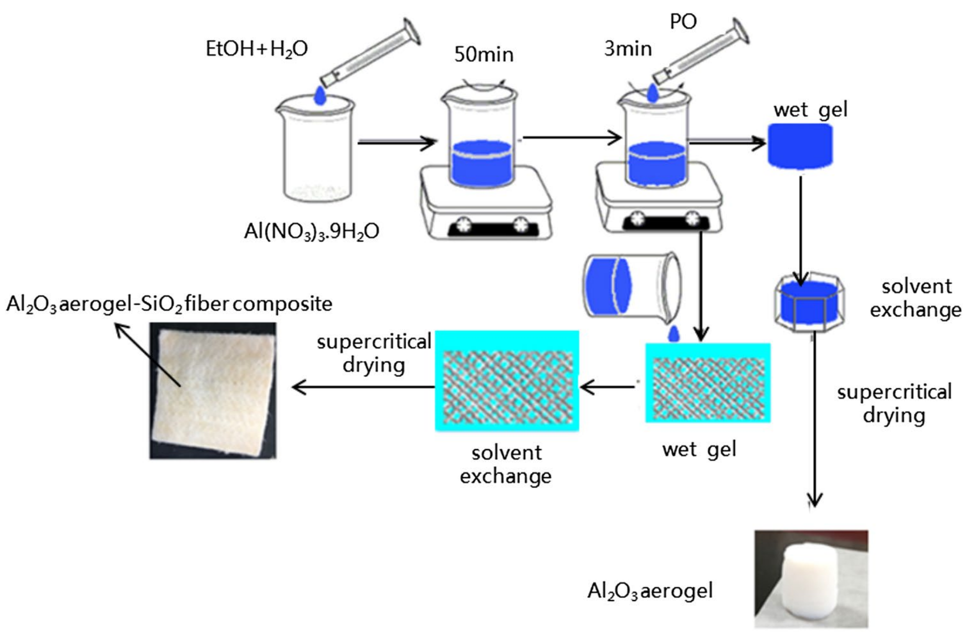

Scheme 1 Schematic illustration of the synthesis processes of pure Al_2O_3 aerogel and Al_2O_3–SiO_2 fiber composite

obtained after supercritical EtOH drying. For the preparation of Al_2O_3 aerogel-SiO_2 fiber composite, after the same precursor preparation, the Al_2O_3 sol was immersed into SiO_2 fiber mat, and the Al_2O_3 aerogel-SiO_2 fiber composite were synthesized after aging, solvent exchange, and EtOH supercritical drying.

2.3 Characterization

The microstructure of pure Al_2O_3 aerogels and Al_2O_3 aerogel-SiO_2 fiber composite was characterized by scanning electron microscopy (SEM, Ultra 55) and transmission electron microscopy (TEM, Libra200). Fourier transform infrared (FTIR, Nicolet 6700 Thermo Fisher) spectroscopy was used to identify the chemical compositions of the aerogels. Nitrogen adsorption–desorption analysis (Quadrasorb SI) at 77 K was used to indicate the specific surface area and pore size distribution of the composite aerogel. The phase of the aerogels was characterized by an X-ray Diffractometer (XRD, X Pert pro). The gas chromatography (GC, Saturn 2100) was used to verify the presence of 1,2-propanediol. Thermal stability analysis was conducted by using thermogravimetry analyzer coupled differential scanning calorimeter (TG-DSC, SDT-600) under a heating rate of 10 °C/min under an air flow. The universal testing machine tested the tensile mechanical properties. The tensile strain rate was set at 3 mm/min for the tests at 25 °C. Thermal conductivity of the composite was measured by using PTF transient automatic measurement at room temperature. Water contact angles (WCAs) on the surface of the composites were measured at an ambient temperature on a contact angle/interface system.

3 Results and discussion

3.1 The characterization and parameters of pure Al_2O_3 aerogels

Scheme S1 exhibited the mechanism of Al_2O_3 gel preparation by using $Al(NO_3)_3·9H_2O$ as the precursor. During the preparation process, the H_2O and EtOH were mixed with the inorganic aluminum salt for the full hydrolysis of $Al(NO_3)_3·9H_2O$. The PO was employed as a coagulant, and it could slowly consume the H_2O in an acidic condition in fact and facilitate the condensation mildly. For $Al(NO_3)_3·9H_2O$ as the aluminum precursor, the aluminum salt was completely hydrolyzed and then PO was added. Thus, the H_2O, $Al(NO_3)_3$, HNO_3, and PO existed in the mixture. PO protonated in an acidic environment firstly then the reaction between water and PO to produce 1,2-propanediol mainly dominate. In order to identify the mechanism of Al_2O_3 gel preparation by using $Al(NO_3)_3·9H_2O$ as the precursor, the exchanged solvent was distilled to gain a mixture of water and alcohols firstly, the water in mixture was removed with anhydrous sodium sulfate, and finally the alcohols were analyzed by gas chromatography. The gas chromatogram (Figure S1) showed that both the standard and sample showed peaks at 12.631 min, which was the characteristic peak of 1,2-propanediol. Thus, the mechanism of Al_2O_3 gel preparation by using $Al(NO_3)_3·9H_2O$ as the precursor was confirmed by gas chromatography. The mechanism of Al_2O_3 gel preparation by using $Al(NO_3)_3·9H_2O$ as the precursor was vertified firstly, which would be meaningful for clear understanding for Al_2O_3 gel preparation and the design of Al_2O_3 aerogel structure–property.

Figure 1 showed XRD patterns of Al_2O_3 aerogels heat-treated at different temperatures. For the as-prepared one, the broad diffraction peak around 2θ = 25° was corresponded to the (110) crystal plane of pseudoboehmite (γ-AlOOH), indicating its amorphous structure [20, 35]. It was seen that the crystal structure of Al_2O_3 aerogels maintained the amorphous structure under the heat-treatment at the temperature below 900 °C. Even after heated at 900 °C for 2 h, the (400) and (440) crystal planes of γ-Al_2O_3 just began to emerge. Compared with other reports (the crystal transfer temperature ~ 700 °C), the crystal transfer temperature from γ-AlOOH to γ-Al_2O_3 was increased as high as 900 °C, which could be attributed that the addition of water made the pore size distribution of the Al_2O_3 aerogels more uniform to form nanocrystals. It was seen that the γ-Al_2O_3 phase still retained after heated at 1100 °C for 2 h [33, 39] and the (311) crystal phase of θ-Al_2O_3 began to appear. It is known that the reducing of thermal resistance for Al_2O_3 aerogels at high temperature was caused by the crystal phase transformation. The higher crystal transfer temperature from the amorphous

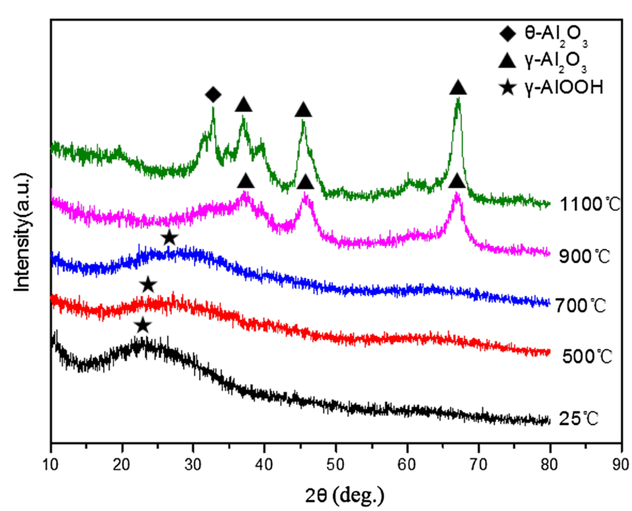

Fig. 1 XRD patterns of Al_2O_3 aerogels heat-treated at different temperatures

to the crystal type meaned the better temperature resistance for Al_2O_3 aerogels. Thus, it could be demonstrated that the Al_2O_3 aerogel prepared in the present work exhibited good temperature resistance with the crystal transfer temperature as high as 900 °C.

Figure 2 showed the FTIR analysis of Al_2O_3 aerogels heated at different temperatures. The absorption bands located at 3433.96 cm^{-1} and 1632.67 cm^{-1} are commonly assigned to the O–H stretching vibration and bending vibration of water molecule, respectively. The absorption bands located at 612.7 cm^{-1} is corresponded to the AlO–H vibration within pseudoboehmite, which is similar to the alumina aerogels reported by Zu et al. [39]. The absorption bands located at 1384.33 cm^{-1} was consistent with the –OH vibration of AlO–H, which proved the maintaining of the amorphous γ-AlOOH. After heated at 900 °C, it disappeared, which was consistent with the XRD pattern [35].

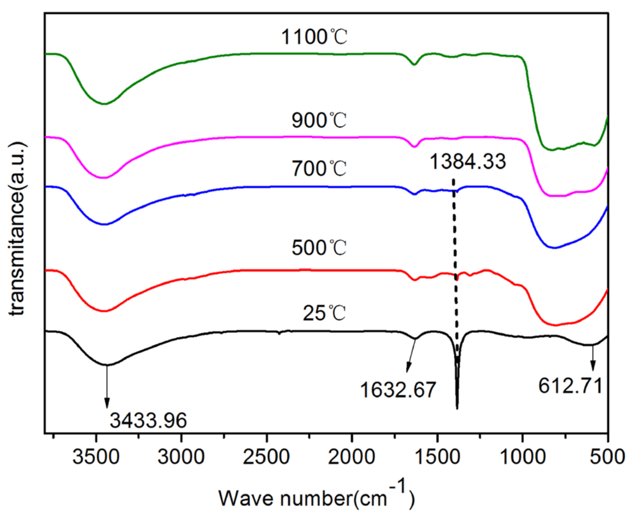

Fig. 2 FTIR spectra of Al_2O_3 aerogels heat-treated at different temperatures

As seen from Fig. 3, it showed SEM and TEM images of the as-prepare Al_2O_3 aerogel and the one after heated at 900 °C. Figure 3a displayed that the microstructure of as-prepared Al_2O_3 aerogel was interpenetrating and it had homogeneous structure with many nanopores. Figure 3b showed that the as-prepared Al_2O_3 aerogel was indeed amorphous structure, which was well consistent with the XRD and FTIR results. Figure 3c showed that after heated at 900 °C, there came particle agglomeration to form large particles in the Al_2O_3 aerogel and the amorphous structure transferred to crystal type. The particle agglomeration caused the reduction of temperature resistance for Al_2O_3 aerogels. According to the analysis of the previous mechanism, Fig. 3a showed that the as-prepared Al_2O_3 aerogel was a material with a three-dimensional network structure formed by fine particles, which was attributed to the water and PO. Since the addition of water allows sufficient hydrolysis and uniform dispersion of the aluminum salt in the mixture, the gelation time is lengthened to increase the size of the particles. But the addition of PO accelerated the gel rate, and the particle size of the obtained particles maitains small. Therefore, the combination of water quantity and PO quantity is an important factor in controlling particle size. Thus, the as-prepared Al_2O_3 aerogel achieved the three-dimensional network structure with small particles, which improved the temperature resistance. Therefore, the thermal insulation and heat resistance of the Al_2O_3 aerogel would endow the Al_2O_3 aerogel-SiO_2 fiber composite excellent performance.

3.2 The characterization and properties of Al_2O_3 aerogel-SiO_2 fiber composite

Figure S2 showed SEM images of the Al_2O_3 aerogel-SiO_2 fiber composite. It could been seen that there was a lot of aerogel particles attached to the fiber. The thermal conductivities of the Al_2O_3 aerogel-SiO_2 fiber composite heated at different temperatures were measured. As seen

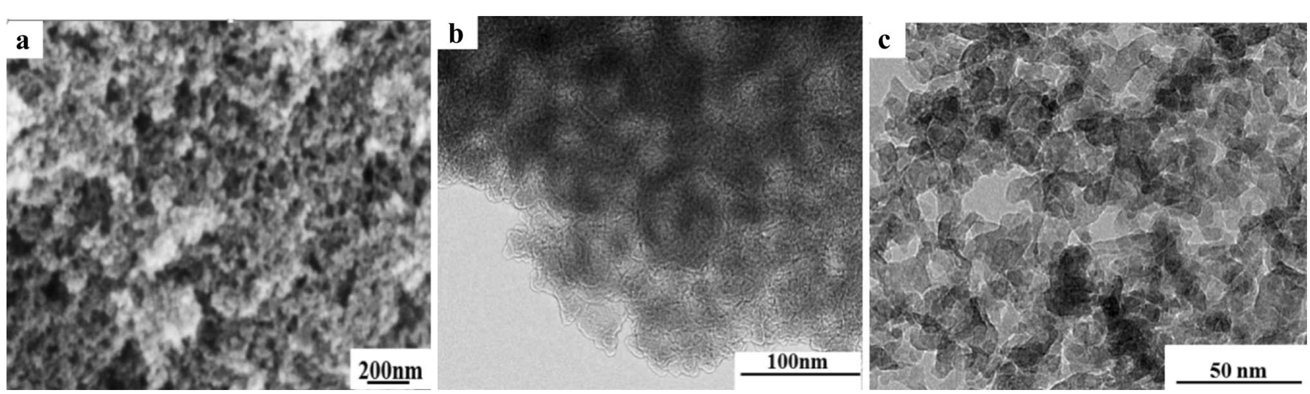

Fig. 3 **a** SEM and **b** TEM images of the as-prepared Al_2O_3 aerogel. **c** TEM image of the Al_2O_3 aerogel heat-treated at 900 °C

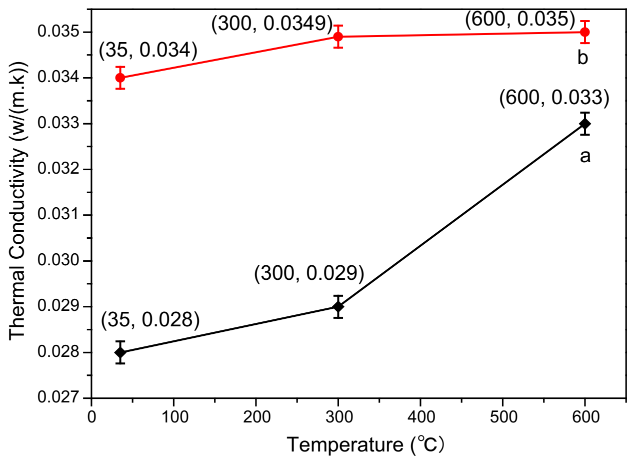

Fig. 4 The thermal conductivities of **a** Al_2O_3 aerogel-SiO_2 fiber composite and **b** SiO_2 fiber mat heat-treated for 2 h at different temperatures

from Fig. 4, it was seen that the thermal conductivity of Al_2O_3 aerogel-SiO_2 fiber composite was 0.028 W/(m K) at 35 °C, compared with that of pure SiO_2 fiber mat at 30 °C (~ 0.034 W/(m K)), and the thermal conductivity of the Al_2O_3 aerogel-SiO_2 fiber composite decreased by 18%. Moreover, its thermal conductivities were still maintained at 0.030 and 0.033 W/(m K) after heated at 300 and 600 °C for 2 h, respectively, compared with those of SiO_2 fiber mat (~ 0.0349 and 0.035 W/(m K)). This clearly demonstrated good temperature resistance of the Al_2O_3 aerogel-SiO_2 fiber composite. N_2 adsorption–desorption isotherms measurement of the Al_2O_3 aerogel-SiO_2 fiber composite was used to characterize the specific surface area and pore structure of the Al_2O_3 aerogel-SiO_2 fiber composite. The specific surface area and pore size distribution of the sample were calculated by using the Brunauer–Emmett–Teller (BET) (Fig. 5). The Al_2O_3 aerogel-SiO_2 fiber composite had the specific surface area of 239.2 m^2/g, pore volume of 0.9 cm^3/g and the main

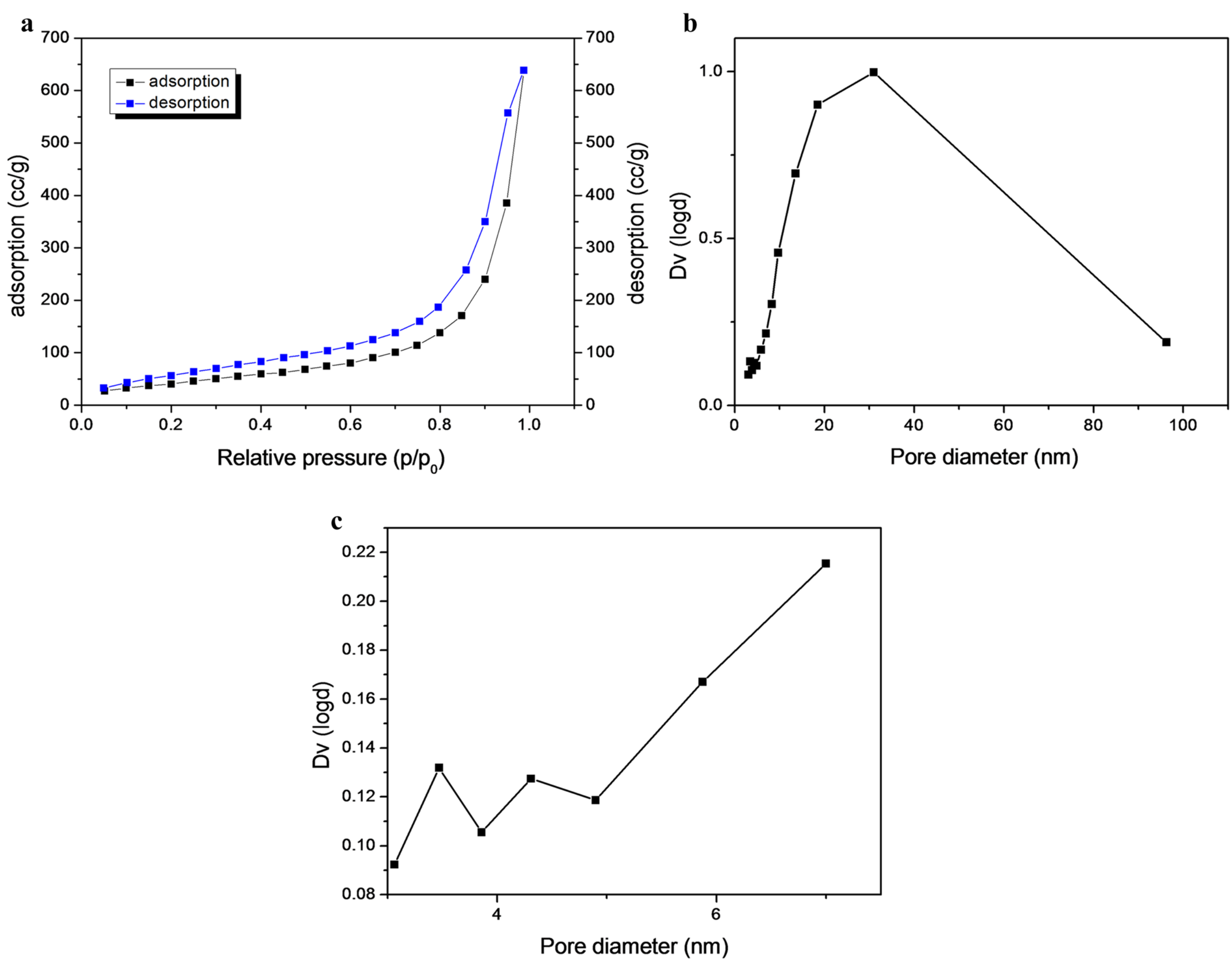

Fig. 5 The N_2 adsorption–desorption isotherms (**a**) and the pore size distribution (**b**) of Al_2O_3 aerogel-SiO_2 fiber composite, **c** is the inserted graph (red circle) of Fig. 5b

pore diameter of 12.7 nm. The composite sample showed the typical IV isotherms according to the IUPAC classification, which is characteristic of the mesoporous structure. Meanwhile, it was seen that there was a broad distribution for the composite sample and the Al_2O_3 aerogel mainly contributed the small grain size, which resulting in good temperature resistance and thermal insulation properties. Besides, Figure S3 showed the TG and DSC curves of the Al_2O_3 aerogel-fiber composite and it was seen that the remaining amount of the Al_2O_3 aerogel-fiber composite was more than 92% at 1200 °C. The TG curve was a detailed description of the process of converting γ-AlOOH to γ-Al_2O_3. The mass of the Al_2O_3 aerogel-SiO_2 fiber composite decreased with increasing temperature in the range of 0 to 300 °C which was due to the loss of surface-adsorbed water and the combined one. The continuous decrease in the mass of the composite from 300 to 1000 °C was caused by the loss of water in the lattice when γ-AlOOH slowly changed to γ-Al_2O_3 with increasing temperature [40–42]. When the temperature raised to 1000 °C, the mass of the composite was no longer reduced, and γ-AlOOH was completely converted into γ-Al_2O_3. Besides, there was an endothermic peak around 1000 °C, which was corresponded to the crystal transformation from γ-AlOOH to γ-Al_2O_3. Figure 1 XRD showed that as the temperature increased, the crystal phase transition temperature of the sample from γ-AlOOH to γ-Al_2O_3 was at 900 °C. However, Figure S3 TGA showed that the phase transition temperature according to the endothermic peak occurred at 1000 °C. The difference between the two temperature could be attributed that the TG analysis has a short-term rapid temperature rise. However, the crystal transition of the sample does not change instantaneously but gradually occurs, and so the crystal transition temperature shows thermal hysteresis and this is a common phenomenon in the TG analysis [43–46]. This indicated that the Al_2O_3 aerogel-fiber composite also had high thermal resistance as well as good thermal insulation. The pore structure of silica fiber mat belongs to the micron level. Due to thermal convection, its thermal conductivity is high. Therefore, the nanostructured Al_2O_3 aerogel was filled in the silica fiber mat to decline the thermal conductivity of the composite. The results showed that Al_2O_3 aerogels had the function of thermal insulation to improve thermal insulating performance of Al_2O_3 aerogel-SiO_2 fiber composite. In a word, it showed that Al_2O_3 aerogel-SiO_2 fiber composite had good thermal insulation and thermal resistance properties [47–49].

Furthermore, as seen from Fig. 6, it could be seen that the mechanical strength, such as the Young's modulus, increased in the case of SiO_2 fiber mat reinforced by Al_2O_3 aerogels. The Al_2O_3 aerogel-SiO_2 fiber composite achieved a higher Young's modulus of tensile strength up to 6.59 MPa than that of the SiO_2 fiber mat (5.79 MPa). The addition of Al_2O_3 aerogels into the fiber mat resulted in the thickened

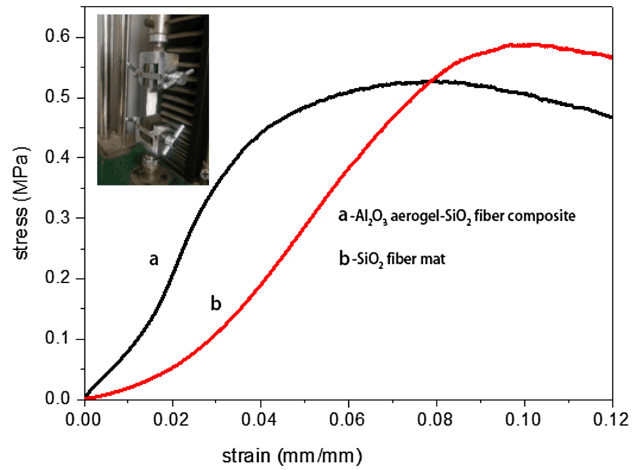

Fig. 6 The strain–stress curves of **a** Al_2O_3 aerogel-SiO_2 fiber composite and **b** SiO_2 fiber mat

skeleton and so improved the tensile strength. Besides, Figure S4 showed that the composite had the hydrophobic property after supercritical EtOH drying and the hydrophobic angle was 136°, which was higher than that of SiO_2 fiber mat (121°). This was because the reaction between hydroxyl group (–OH) on the surface of Al_2O_3 gel and alcohol resulted in the substitution of hydroxyl group by the hydrophobic –C_2H_5 group on the surface of Al_2O_3 aerogels. Therefore, the Al_2O_3 aerogel-SiO_2 fiber composite had a hydrophobicity, suggesting its humidity resistance property.

As seen from Table S1, the Al_2O_3 aerogels were introduced into the SiO_2 fiber mat to improve the thermal insulation performance and the Al_2O_3 aerogel-SiO_2 fiber composite had low thermal conductivity (0.028 W/(m K)) at 35 °C, which was lower than that of Al_2O_3–SiO_2 aerogel/zirconia ceramics composite (0.049 W/(m K)) at 35 °C [38]. Besides, the Al_2O_3 aerogel-SiO_2 fiber composite had low thermal conductivity (0.029 W/(m K)) at 300 °C, which was lower than that of Al_2O_3–SiO_2 aerogel/Mullite fiber mat composite (0.032 W/(m K)) at 300 °C [50]. Meanwhile, the Al_2O_3 aerogel-SiO_2 fiber composite showed the higher mechanical property than Al_2O_3–SiO_2 aerogel/Mullite fiber [37]. As a result, the enhanced thermal insulation and high heat resistance would endow Al_2O_3 aerogel-SiO_2 fiber composites with well actual application in future.

4 Conclusion

In this work, the thermal-resistance Al_2O_3 aerogels were prepared by the sol–gel method, followed by aging, solvent exchange and supercritical drying. This work was the first proved the mechanism of Al_2O_3 gel preparation by using $Al(NO_3)_3·9H_2O$ as the precursor, which would be meaningful for clear understanding for Al_2O_3 gel preparation and the design of Al_2O_3 aerogel structure–property. Moreover, due to the addition of water for making the uniform pore structure and nanocrystals of the Al_2O_3 aerogels, the crystal phase transition from γ-AlOOH to γ-Al_2O_3 occurred within the Al_2O_3 aerogels as high as 900 °C. The result showed that the Al_2O_3 aerogels had a high crystalline phase transition temperature. Inspired by this, the Al_2O_3 aerogels were introduced into the SiO_2 fiber mat to improve the thermal insulation performance. As a result, the Al_2O_3 aerogel-SiO_2 fiber composite had low thermal conductivity (0.028 W/(m K) at 35 °C and 0.033 W/(m K) after heated at 600 °C), high thermal stability, mechanical property (the Young's modulus of tensile strength up to 6.59 MPa) and the hydrophobic property (~ 136°). Thus, due to low thermal resistance, high thermal stability and good humidity resistance, the Al_2O_3 aerogel-SiO_2 fiber composite would have good thermal insulation performance in future.

Acknowledgements This research was financially supported by Sichuan Science and Technology Program (No. 2018RZ0127), the Project of State Key Laboratory of Environment-friendly Energy Materials, Southwest University of Science and Technology (Nos. 17FKSY0111 and 18zxhk16) and the Doctoral Research Fund of Southwest University of Science and Technology (No. 16zx7142).

Compliance with ethical standards

Conflict of interest The authors declare that they have no competing interest.

References

1. L. Sorensen, G.F. Strouse, A.E.J.AM. Stiegman, Fabrication of stable low-density silica aerogels containing luminescent ZnS capped CdSe quantum dots. Adv. Mater. **18**, 1965–1967 (2010)
2. S. Zhao, Z. Zhang, G. Sèbe, R. Wu, R.V.R. Virtudazo, P. Tingaut, M.M. Koebel, Multiscale assembly of superinsulating silica aerogels within silylated nanocellulosic scaffolds: improved mechanical properties promoted by nanoscale chemical compatibilization. Adv. Funct. Mater. **25**, 2326–2334 (2015)
3. L. Li, B. Yalcin, B.N. Nguyen, M.A. Meador, Cakmak and interfaces, flexible nanofiber-reinforced aerogel (xerogel) synthesis, manufacture, and characterization. ACS App. Mater. Interfaces **1**, 2491 (2009)
4. J.H Robinson, Orbital debris impact damage to reusable launch vehicles. Int. J. Impact Eng **23**, 783–794 (1998)
5. R.G. Martinez, E. Goiti, G. Reichenauer, S. Zhao, M. Koebel, Barrio and buildings, thermal assessment of ambient pressure dried silica aerogel composite boards at laboratory and field scale. Energy Buildings **128**, 111–118 (2016)
6. H. Yamashita, T. Ogami, K. Kanamura, Hydrothermal synthesis of hollow Al_2O_3 microfibers for thermal insulation materials. Bull. Chem. Soc. Jpn. **91**, 741–746 (2018)
7. G. Wang, J. Zhao, H.M. Lun, G. Wang, K. Yu, C. Wang, C.B. Park, G.J. Zhao, Ultra-tough and super thermal-insulation nanocellular PMMA/TPU. Chem. Eng. J. **325**, 632–646 (2017)
8. A.M. Abraham, S.V. Kumar, S.M. Alhassan, A.M. Abraham, S.V. Kumar, S.M. Alhassan, Porous sulphur copolymer for gas-phase mercury removal and thermal insulation. Chem. Eng. J. **332**, 1–7 (2018)
9. B. Wang, Y.R. Wang, Effect of fiber diameter on thermal conductivity of the electrospun carbon nanofiber mats. Adv. Mater. Res. **332–334**, 672–677 (2011)
10. A.R. Bunsell, M.H. Berger, Fine diameter ceramic fibres. J. Eur. Ceram. Soc. **20**, 2249–2260 (2000)
11. C. Simón-Herrero, A. Romero, J.L. Valverde, L.J.J. Sánchez-Silva, Hydroxyethyl cellulose/alumina-based aerogels as lightweight insulating materials with high mechanical strength. J. Mater. Sci. **53**, 1556–1567 (2018)
12. Q.F. Xu, H.B. Ren, J.Y. Zhu et al., Facile fabrication of graphite-doped silica aerogels with ultralow thermal conductivity by precise control. J. Non-Cryst. Solids **469**, 14–18 (2017)
13. X. Lu, M.C. Arduini-Schuster, J. Kuhn, O. Nilsson, J. Fricke, R.W. Pekala, Thermal conductivity of monolithic organic aerogels. Science **255**, 971–972 (1992)
14. T.Y. Wei, T.F. Chang, S.Y. Lu, A.C.S. Chang, Preparation of monolithic silica aerogel of low thermal conductivity by ambient pressure drying. J. Am. Ceram. Soc. **90**, 2003–2007 (2010)
15. L.J. Wang, S.Y. Zhao, M. Yang, Structural characteristics and thermal conductivity of ambient pressure dried silica aerogels with one-step solvent exchange/surface modification. Mater. Chem. Phys. **113**, 485–490 (2009)
16. L. Hrubesh, Aerogel applications. J. Non-Cryst. Solids **225**, 335–342 (1998)
17. S. Keshipour, M.J.C. Khezerloo, Au-dimercaprol functionalized cellulose aerogel: synthesis, characterization and catalytic application: Heterogeneous biocatalysis. Appl. Organomet. Chem. **32**, e4255 (2018)
18. Y. Fu, G. Wang, X. Ming, X. Liu, B. Hou, T. Mei, J. Li, J. Wang, X.J.C. Wang, Oxygen plasma treated graphene aerogel as a solar absorber for rapid and efficient solar steam generation. Carbon **130**, 250–256 (2018)
19. N. Nazeran, S. J.J.J.o.N.-C, Moghaddas, Synthesis and characterization of silica aerogel reinforced rigid polyurethane foam for thermal insulation application. J. Non-Cryst. Solids **461**, 1–11 (2017)
20. F. Cao, L. Ren, X.J. Li, Synthesis of high strength monolithic alumina aerogels at ambient pressure. Res. Adv. **5**, 18025–18028 (2015)
21. A.C. Pierre, G.M. Pajonk, Chemistry of aerogels and their applications. Chem. Rev. **34**, 4243–4265 (2002)
22. J.P. Randall, M.A.B. Meador, S.C. Jana, Tailoring mechanical properties of aerogels for aerospace applications. ACS App. Mater. Int. **3**, 613–626 (2011)
23. S.S. Prakash, C.J. Brinker A.J.J. Hurd, Silica aerogel films at ambient pressure. J. Non-Cryst. Solids **190**, 264–275 (1995)
24. F. Shi, L. Wang, J. Liu, Synthesis and characterization of silica aerogels by a novel fast ambient pressure drying process. Mater. Lett. **60**, 3718–3722 (2006)
25. N. Hüsing, U.J.A.C.I.E. Schubert, Aerogels—airy materials: chemistry, structure, and properties. Angew. Chem. Int. Ed. **37**, 22–45 (1998)
26. X. Du, F. Kleitz, X. Li, H. Huang, X. Zhang, S.Z.J.A.FM. Qiao, Disulfide-bridged organosilica frameworks: designed, synthesis, redox-triggered biodegradation, and nanobiomedical applications. Adv. Funct. Mater. **28**, 1707325 (2018)
27. X. Du, X. Li, L. Xiong et al., Mesoporous silica nanoparticles with organo-bridged silsesquioxane framework as innovative platforms for bioimaging and therapeutic agent delivery. Biomaterials **91**, 90–127 (2016)

28. S. Komarneni, R. Roy, U. Selvaraj, P.B. Malla, Research, nanocomposite aerogels: the SiO_2–Al_2O_3 system. J. Mater. Res. **8**, 3163–3167 (1993)
29. M. Li, H. Jiang, D. Xu et al., Low density and hydrophobic silica aerogels dried under ambient pressure using a new co-precursor method. J. Non-Cryst. Solids **452**, 187–193 (2016)
30. X. Ji, Q. Zhou, G. Qiu, B. Peng, M. Guo, M.J.S. Zhang, Synthesis of an alumina enriched Al_2O_3-SiO_2 aerogel: Reinforcement and ambient pressure drying. J. Non-Cryst. Solids **471**, 160–168 (2017)
31. J.F. Poco, N.-C.S. Hrubesh, Synthesis of high porosity, monolithic alumina aerogels. J. Non-Cryst. Solids **285**, 57–63 (2001)
32. T.F. Baumann, A.E. Gash, S.C. Chinn, A.M. Sawvel, R.S. Maxwell, J.H.S. Satcher, Synthesis of high-surface-area alumina aerogels without the use of alkoxide precursors. Chem. Mater. **17**, 395–401 (2005)
33. S. Zhang, W. Cai, J. Yu et al., A facile one-pot cation-anion double hydrolysis approach to the synthesis of supported MgO/γ-Al_2O_3 with enhanced adsorption performance towards CO_2. Chem. Eng. J. **310**, 216–225 (2017)
34. G. Zu, J. Shen, X. Wei, X. Ni, Z. Zhang, J. Wang, Preparation and characterization of monolithic alumina aerogels. J. Non-Cryst. Solids **357**, 2903–2906 (2011)
35. L. Xu, Y. Jiang, J. Feng et al., Infrared-opacified Al_2O_3–SiO_2, aerogel composites reinforced by SiC-coated mullite fibers for thermal insulations. Ceram. Int. **41**, 437–442 (2015)
36. R. Zhang, N. Jiang, X.J. Duan et al., Synthesis and characterization of Al_2O_3–SiO_2 hybrid aerogels by a one-pot sol–gel method. New Carb. Mater. **32**, 258–264 (2017)
37. X. Wu, G. Shao, S. Cui, L. Wang, X.J.C.I. Shen, Synthesis of a novel Al_2O_3–SiO_2 composite aerogel with high specific surface area at elevated temperatures using inexpensive inorganic salt of aluminum. Ceram. Int. **42**, 874–882 (2016)
38. R. Zhang, C. Ye, B. Wang, Novel Al_2O_3-SiO_2, aerogel/porous zirconia composite with ultra-low thermal conductivity. J. Porous Mater. **25**, 171–178 (2018)
39. G. Zu, J. Shen, L. Zou, W. Wang, Y. Lian, Z. Zhang, Nanoengineering super heat-resistant, strong alumina aerogels. Chem. Mater. **25**, 4757–4764 (2013)
40. J.T. Zhang, J.W. Jiang, C.C. Zhao, Synthesis and capacitive properties of manganese oxide nanosheets dispersed on functionalized graphene sheets. J. Phys. Chem. C **115**, 6448–6454 (2011)
41. M.M. Liu, J.C. Liu, M.C. Wang, Z.Q.J. Yun, Preparation and properties of SiO_2/Al_2O_3–SiO_2 fiber mat composite materials. Key Eng. Mater. **680**, 129–132 (2016)
42. J. Liu, H. Xu, W. Shen, X. Pan, Y.J.J.T.A. Xiang. Calorimetry, TG study of the dispersion threshold of Mn_2O_3 on γ-Al_2O_3. J. Therm. Anal. Calorim. **58**, 309–315 (1999)
43. Y.M. Kim, G.H. Rhee, C.H. Ko, K.H. Kim, K.Y. Jung, J.M. Kim. Park and nanotechnology, catalytic pyrolysis of *Pinus densiflora* over mesoporous Al_2O_3 catalysts. J. Nanosci. Nanotechol. **18**, 6300–6303 (2018)
44. C. Wu, W. Yuan, Y. Huang, Y. Xia, H. Yang, H. Wang, X.J.C.L. Liu, Conversion of xylose into furfural catalyzed by bifunctional acidic ionic liquid immobilized on the surface of magnetic γ-Al. Catal. Lett. **147**, 953–963 (2017)
45. X. Wang, J. Wang, H.J.J.o.MP. Wang, A heat-resistant organic adhesive for joining Al_2O_3 ceramics in air and argon atmospheres. J. Manuf. Process. **26**, 67–73 (2017)
46. H.B. Zhao, M. Chen, H.B. Chen, Thermally insulating and flame-retardant polyaniline/pectin aerogels. ACS Sustainable Chem. Eng. **5**, 7012–7019 (2017)
47. M. Yao, N. Wang, W. Hu et al., Novel hydrothermal electrodeposition to fabricate mesoporous film of $Ni_{0.8}Fe_{0.2}$, nanosheets for high performance oxygen evolution reaction. Appl. Catal. B. **233**, 226–233 (2018)
48. N. Wang, B. Sun, P. Zhao, M. Yao, W. Hu, S.J.C.E.J. Komarneni, Electrodeposition preparation of $NiCo_2O_4$ mesoporous film on ultrafine nickel wire for flexible asymmetric supercapacitors. Chem. Eng. J. **345**, 31–38 (2018)
49. N. Wang, H.D. Song, H.B. Ren, J.Y. Chen, M.Q. Yao, W.Y. Huang, W.C. Hu, Komarneni partly nitrogenized nickel oxide hollow spheres with multiple compositions for remarkable electrochemical performance. Chem. Eng. J. **358**, 531–539 (2019)
50. H. Chen, X.Y. Sui, C.L. Zhou et al., Preparation and characterization of mullite fiber-reinforced Al_2O_3–SiO_2 aerogel composites. Key Eng. Mater. **697**, 360–363 (2016)